

Quantum Coherence of Image Potential States

P. Wahl, M.A. Schneider, L. Diekhöner, R. Vogelgesang, and K. Kern

Max-Planck-Institut für Festkörperforschung, Heisenbergstr. 1, D-70569 Stuttgart, Germany

(Dated: March 2, 2019)

The quantum dynamics of the two-dimensional electron gas (2DEG) formed by the image potential states in front of the Cu(100) surface is measured by scanning tunneling microscopy (STM) and spectroscopy (STS). The dispersion relation and the momentum resolved phase-relaxation time of the first image potential state are determined from the quantum interference patterns in the local density of states (LDOS) at step edges. It is demonstrated that the tip-induced Stark shift does not affect the motion of the electrons parallel to the surface.

PACS numbers: 73.20.At, 68.37.Ef, 72.15.Lh, 72.10.Fk

The image potential states are model states for the study of electronic interactions of electrons at surfaces, a topic that has far reaching consequences for many surface processes. The self interaction of electrons near metallic surfaces gives rise to eigenstates which are confined along the surface normal by the classical image potential on the vacuum side of the crystal surface and by the band structure of the crystal on the other side [1]. The lifetime of electrons injected or excited into an image state is limited mainly by their interaction with bulk electrons. This has been studied in great detail in recent years by energy- and time-resolved two-photon photoemission spectroscopy (2PPE) [2, 3, 4, 5]. Theoretical understanding of the involved electron-electron scattering processes has established that the lifetime of image-state electrons is determined by interband scattering with bulk electrons and by intraband contributions [3, 6].

The high LDOS of the image states near the surface makes them accessible to STM. They appear at rather high sample bias voltages of 4–8V. The electric field between tip and sample induces a Stark shift of the eigenenergies to higher values. Interest in image states modified by the presence of an STM tip has focused so far on the fact that the energetic positions of the states are sensitive to the electronic structure of the surface [7, 8]. Spectroscopy of image states by STM has been used to achieve chemical contrast on the nanometer scale for metals on metal surfaces, e.g. Cu on Mo(110) [8] or Fe/Cr surface alloys [9].

In this letter, we present for the first time STM measurements of the properties of the 2DEG formed by the image potential states in front of the surface. Due to elastic scattering at point defects and step edges of the electrons injected into these states, modulations of the LDOS emerge. Using STS, we determine the binding energies for the first four image states as well as the dispersion relation and the phase coherence length of the $n = 1$ Stark-shifted image state on Cu(100). This opens up the possibility to study these quantities locally in nanostructures. In the case of surface state electrons at metal surfaces the local dynamics has been studied by STS in great detail [10, 11, 12, 13]. The results show a good

agreement between photoemission and STS experiments on the one side and theory on the other side [12, 13]. A similar comparison is missing in the case of image states.

We used a Cu(100) single crystal sample, carefully prepared by sputtering and annealing cycles in UHV (base pressure $1 \cdot 10^{-10}$ mbar). After cleaning the sample was transferred *in situ* into a home-built STM operating at 6K. Spectroscopic measurements were performed using a lock-in technique with a modulation of the sample voltage of 10–30mV_{RMS} at a frequency of 4.5kHz. All bias voltages U are sample potentials measured with respect to the tip.

Fig. 1(a) shows a typical STM image of an artificially created step edge. The upper half is a topographic image and the lower half shows the simultaneously acquired dI/dV -map taken at the same bias voltage. It reveals the quantum interference pattern of the $n = 1$ image state created by elastic scattering of the electrons injected by the tip into the image state. We will later present a detailed analysis of these patterns leading to the dispersion relation and the momentum resolved linewidth of the $n = 1$ Stark-shifted image state.

The binding energies of the Stark-shifted image states can be measured using $z(V)$ spectroscopy as shown in Fig. 1(b). For this experiment the feedback loop is kept active while sweeping the bias voltage. To maintain a constant current the tip is retracted with increasing bias voltage as more and more states become available to the tunneling electrons. We have taken $z(V)$ -spectra at currents of 0.1 to 1nA. The spectra show a series of steps, where each step is due to the contribution of a new image state to the tunneling current allowing us to identify the first four image states. Their binding energies E_n relative to the vacuum level E_{vac} of the sample are obtained from the bias voltages U_n , at which the steps occur by

$$E_n = eU_n - \phi \quad (1)$$

where $\phi = 4.6\text{eV}$ [5] is the work function of Cu(100) and e the elementary charge. Below 3V there are no further image states therefore the step at $U = 4.7\text{V}$ is clearly identified as the state $n = 1$. As can be seen from a comparison of the two spectra shown in Fig. 1(b), the

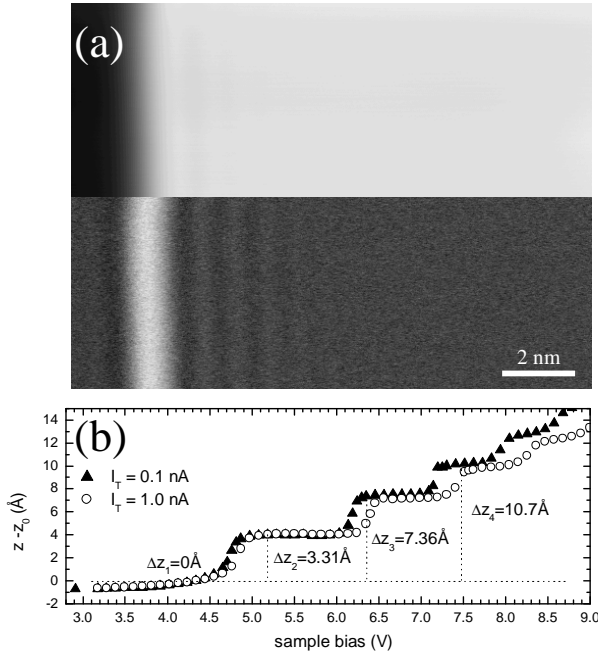


FIG. 1: (a) Upper half: STM topography of an artificially created step on Cu(100) taken at 5.2V bias voltage, lower half: dI/dV -map of the same place at the same bias voltage. The image state electrons reflected at the step edge create a density modulation which appears as a standing wave pattern in the dI/dV -map. (b) Measured $z(V)$ curve on a terrace of Cu(100) using two different tunneling currents of 0.1 and 1.0nA. We observe up to four image states in the electric field of the STM tip. The measured increments in the tip-sample distance are labelled Δz_n .

states shift to higher binding energies for higher tunneling currents due to the decreased tip-sample distance. The binding energies are considerably larger compared to the undisturbed states which form a Rydberg series at negative binding energies starting at -0.6eV with respect to E_{vac} [3, 14]. Also, due to the electric field in the tunneling gap the energetic distance between the states is enlarged facilitating the separate spectroscopy of higher order states [7].

To analyze these findings we performed model calculations using a one-dimensional potential as introduced by Chulkov et al. [14]. This potential reproduces the Rydberg series of the image states and the positions of the projected band edges at the $\bar{\Gamma}$ point ($k_{||} = 0$) in the Cu(100) surface Brillouin zone. We integrated the Schrödinger equation in real space employing the model potential for a 25 layer crystal. The influence of the tip is modelled by adding as function of the bias voltage a linearly increasing potential to the image potential of the crystal reaching from the point z_{im} (see Ref. 14) to the point $z_{\text{im}} + z$ where z is the tip-sample distance which is treated as an adjustable parameter (see Fig 2(a), a similar ansatz has been used in Ref. 15). In such a simple

model, the binding energies of the image states in the electric field of the STM tip are reproduced.

The model potential and the probability distribution of the resulting wave function are shown in Fig. 2(a). Fig 2(b) shows schematically the resulting energy level diagram. It is clear that the presence of the tip reduces the spatial extent of the electronic states considerably (c.f. Fig. 6 of Ref. 14) hence the energetic shift of the states. This is shown in Fig. 2(c), where the calculated binding energies E_n of the image states are plotted as a function of the applied bias voltage for the measurement with a tunneling current of 0.1nA. In the limit of vanishing electric field the calculations yield the binding energies of the undisturbed image states. For each state n a different tip sample distance $z = \Delta z_n + z_0$ was used, where Δz_n is given by the measured plateaus in Fig. 1(b) and $z_0 = 22.5\text{\AA}$. This reflects the fact that

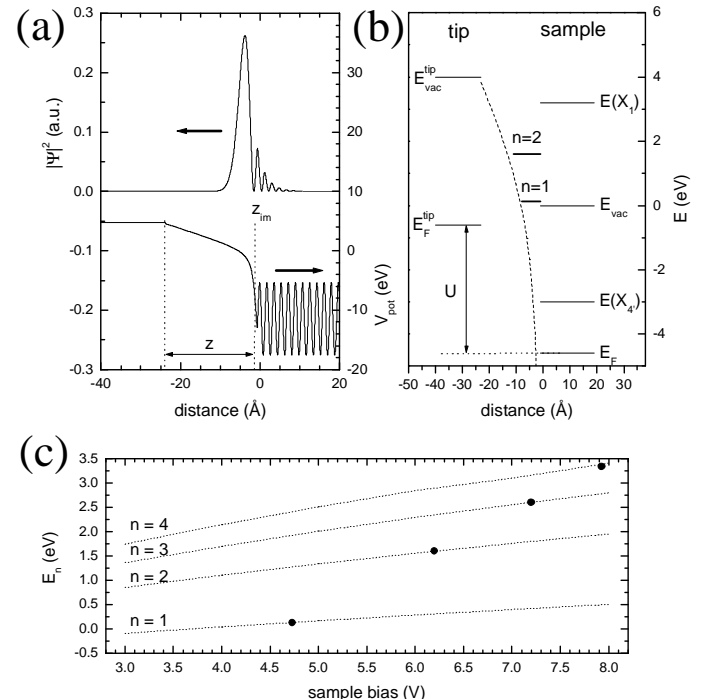


FIG. 2: (a) one-dimensional model potential used and probability density of the wave function of the first image state obtained. (b) schematic drawing of the energy levels of the resonances, the Fermi levels of tip and sample, the bulk band edges of the Cu(100) crystal ($E(X_4')$ and $E(X_1)$) and the potential in the tunneling gap (dashed line). (c) calculation (dotted lines) of the binding energies of the image states in the electric field of the STM tip as function of the applied voltage. Each of the dotted lines corresponds to one particular state ($n = 1$ to 4) calculated for a tip-sample distance $z = \Delta z_n + z_0$, where Δz_n is taken from the measurement shown in Fig. 1(b) and $z_0 = 22.5\text{\AA}$. Full circles are plotted at the voltages where the steps in Fig. 1(b) occur and at the corresponding energies according to Eq. 1.

tion of an image state the field strength for the following state is decreased through the increase of the tip sample distance (Fig. 1(b)). The positions of the measured steps in Fig. 1(b) are translated into binding energies of the image states by Eq. 1 and plotted as full circles in Fig. 2(c). The agreement is excellent. As expected, the calculation of the energy levels for the measurement at the higher tunneling current of 1nA yields a lower height of the tip above the surface of $z_0 = 19.5\text{\AA}$.

Measurements with different tips, where different means that the tip has been modified by field emission and gentle dipping into the surface, reveal a dependence of the energy levels on the tip properties which is stronger for the higher states. While the $n = 1$ state remains at a bias voltage of $4.7 \pm 0.1\text{V}$, we observe the higher states to shift by as much as 0.5V ($n = 2$) and 0.9V ($n = 3$). This yields a much stronger dependence of the energy levels on tip properties than on tunneling conditions, i.e the current at which the $z(V)$ spectroscopy is performed.

The calculated z_0 values for the tip sample distance at energies below the first resonance appear relatively large judging from a tip height above the surface of 8 to 10\AA on metals with the tunneling currents used here [16]. This may be due to the approximations made in the calculation. The different work functions of tip and sample will introduce a contact potential, which modifies the electric field in the junction. From the experimental point of view it is quite possible that the tungsten tip is coated with copper, since it is frequently prepared by slightly dipping it into the surface. Both, the composition and the morphology of the very end of the tip can lead to a lower work function compared to that of the Cu(100) surface, which allows to reduce z_0 . The potential presented in Fig 2(a) also neglects the image potential at the surface of the tip. Calculations using two Cu(100) model potential surfaces facing each other yield z_0 values which are 3 – 5\AA lower than the ones presented above. Finally, the one dimensional model approximates the tip as a plate. To assess the possible influence of the sharpness of the tip, we have determined the electric field between a sphere and a metal plate and used the resulting potential in the calculations. For a small radius of curvature R of the tip the potential in the tunneling gap will fall off more quickly in the vicinity of the tip compared to the linear potential. However, this effect will only modify the field within the gap if R is comparable to or smaller than the tip-sample distance z . For a reasonable R , the influence of the tip shape on the electric field in the tunneling gap can be neglected. In general, z_0 should rather be interpreted as an effective position, producing a given field strength of the order of 10^9V/m locally, than as the distance between the last tip atom and the surface. Our analysis indicates that the variations of the binding energies of the Stark-shifted image states obtained with different tips are more likely determined by the contact potentials present than by the radius of curvature of the

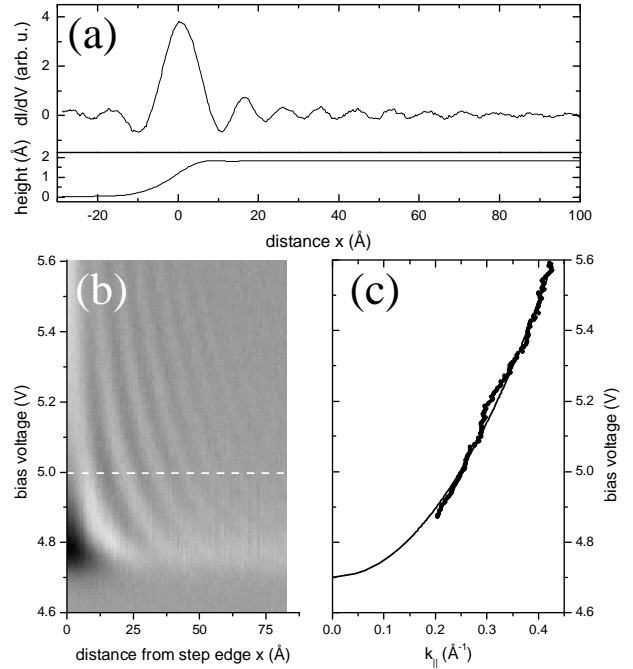


FIG. 3: (a) dI/dV signal at 5.0V sample bias (upper graph) and topographic signal at a step edge. Electron interference produces the oscillations in dI/dV . (b) $dI/dV(V, x)$ -map. dI/dV is plotted a function of the lateral distance x from a step edge and of the bias voltage V [17]. Horizontal line cuts reveal the standing waves due to the interference of electrons in the image state scattered at the step edge. The dashed line indicates the energetic position of the data shown in (a). (c) points represent the k -values obtained from a fit to each line in (b), the solid line shows the parabolic dispersion fitted to these points.

tip. We note that the change in the energetic position of the first resonance with the applied field is comparatively small making it relatively robust against tip changes as observed experimentally, too.

In the following, the dynamical properties of the 2DEG formed by the image state electrons in front of the surface will be discussed in detail. Due to elastic scattering of these electrons at point defects and step edges, modulations of the LDOS are created through quantum interference (Fig. 1(a) and Fig. 3(a)). This allows to study the dynamics of the states with non-vanishing momentum parallel to the surface locally. The analysis of the interference pattern of electrons scattered at a step edge enables the determination of their wave vector and phase coherence length at a given energy. The interference pattern is measured through the dI/dV signal which is proportional to the LDOS at the given energy. In Fig. 3(b) $dI/dV(V, x)$ is measured for bias voltages ranging from 4.6V to 5.6V at increasing distances x from the step edge. The resulting curves are represented as a grey scale map, where horizontal line sections are the energy resolved electron density oscillations as shown in

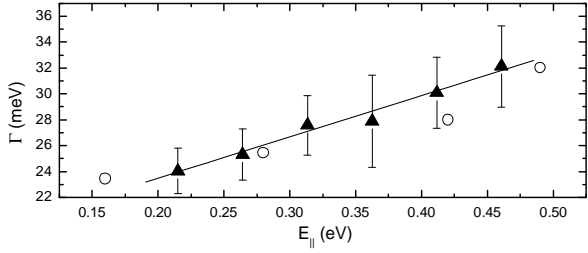


FIG. 4: Phase coherence lengths of the interference pattern at a step edge converted into linewidths $\Gamma(E)$. Solid symbols are the data taken by STM, the solid line is a linear fit to them; open symbols represent linewidths determined by 2PPE measurements from Ref. 3.

Fig. 3(a). The density oscillations reveal the parabolic dispersion relation of the state with $E'_{\Gamma} = 4.7 \pm 0.1$ eV and $m' = (0.8 \pm 0.1)m_0$ (Fig 3(c)). However, with the help of the calculations presented above, the influence of the tip on the dispersion of the image potential state can be corrected for. Since the data are collected in open feedback mode, i.e. the distance between tip and sample is kept constant, one needs only to compensate for the shift of the binding energy at Γ with changing electric field during the bias voltage sweep. The dependence of the state's binding energy on the applied bias voltage close to E'_{Γ} is approximately linear. From the calculations shown in Fig. 2(c) we get $dE_1/dU = 0.12$. Using this correction, we obtain an effective mass of $m^* = m'/(1 - 0.12) = (0.9 \pm 0.1)m_0$. This agrees perfectly with the effective mass $m^* = 0.9m_0$ of the $n = 1$ image state as determined by 2PPE [5].

The standing wave pattern decays with increasing distance from the step edge due to geometric factors and to a loss of coherence [11]. The decaying LDOS pattern in the 2DEG of the image states near a step edge can be described by

$$\rho \approx L_0 \left(1 - r e^{-2x/L_{\Phi}} J_0(2k_{\parallel}x) \right) \quad (2)$$

where L_0 is an overall proportionality constant, r the reflectivity of the step edge, L_{Φ} the phase coherence length, k_{\parallel} the wave vector of the electron parallel to the surface plane, and J_0 the Bessel function of zeroth order.

To determine the lifetime of an electron in the $n = 1$ image state we have analyzed quantitatively the quantum interference pattern and measured the phase coherence length L_{ϕ} as a function of energy on large defect free terraces. The scattering processes thus studied are those experienced in the absence of any defects [11, 13]. Inelastic scattering at the step edge leads to a reduced overall amplitude of the standing waves described by r in Eq. 2. Care was taken to account for instrumental broadening through the applied bias modulation when measuring the dI/dV signal which also induces a decay of the wave pattern [11]. The obtained phase coher-

ence lengths of $75 - 85$ Å are converted into linewidths through $\Gamma(E) = \hbar v(E)/L_{\phi}(E)$ by using the group velocity $v(E)$ determined from the dispersion relation. The results shown in Fig. 4 agree excellently with the k -resolved linewidths found by 2PPE measurements [3]. In agreement with theory, we find $\Gamma(E)$ to increase linearly with energy, although the rate of $d\Gamma/dE = 32$ meV/eV obtained from the fit in Fig. 4 is lower than the theoretical prediction [3]. The comparison of our results with the 2PPE measurements demonstrates that the presence of the tip does not alter substantially the dynamical properties of the 2DEG. Although the state shifts by as much as 0.6 eV due to the presence of the electric field, it is still located near the center of the ~ 6 eV wide directional band gap of Cu(100). There is thus no significant change in the coupling to the bulk electrons, which is the main contribution to the linewidth.

In conclusion, we observed for the first time density modulations of image state electrons in the vicinity of steps and point defects on Cu(100). The quantum interference patterns allow us to determine the dispersion relation of the states which experience a Stark shift due to the electric field in the tunneling junction. Furthermore we measured the phase coherence length of the electrons on clean terraces. Both, the dispersion relation and the phase coherence length agree well with the results of non-local photoemission experiments. This shows that the motion of the electrons parallel to the surface is not noticeably affected by the field of the STM tip. Due to the local character of the measurement the STM can therefore be used to study the dynamical behavior of image-state electrons confined laterally to nanostructures and to characterize the scattering properties of surface defects and adsorbates.

- [1] P.M. Echenique and J.B. Pendry, *J. Phys. C* **11**, 2065 (1978).
- [2] U. Höfer *et al.*, *Science* **277**, 1480 (1997).
- [3] W. Berthold *et al.*, *Phys. Rev. Lett.* **88**, 056805 (2002).
- [4] Ch. Reuß *et al.*, *Phys. Rev. Lett.* **82**, 153 (1999).
- [5] Th. Fauster and W. Steinmann, in *Photonic Probes of Surfaces*, edited by P. Halevi (North Holland, Amsterdam, 1995), pp. 347-411.
- [6] E. V. Chulkov *et al.*, *Phys. Rev. Lett.* **80**, 4947 (1998).
- [7] G. Binnig *et al.*, *Phys. Rev. Lett.* **55**, 991 (1985).
- [8] T. Jung, Y. W. Mo, and F. J. Himpsel, *Phys. Rev. Lett.* **74**, 1641 (1995).
- [9] Y.J. Choi *et al.*, *Phys. Rev. B* **59**, 10918 (1999).
- [10] J. Li *et al.*, *Phys. Rev. Lett.* **81**, 4464 (1998).
- [11] L. Bürgi, O. Jeandupeux, H. Brune, and K. Kern, *Phys. Rev. Lett.* **82**, 4516 (1999).
- [12] J. Kliewer *et al.*, *Science* **288** (5470), 1399 (2000).
- [13] L. Vitali *et al.*, *Surf. Sci.* **523**, L47 (2003).
- [14] E.V. Chulkov, V.M. Silkin, P.M. Echenique, *Surf. Sci.* **437**, 330 (1999)..
- [15] L. Limot *et al.*, cond-mat/0301568 (unpublished).

[16] J.K. Gimzewski and R. Möller, Phys. Rev. B **36**, 1284 (1987).

[17] To enhance the contrast, the average value of each horizontal line has been subtracted.